Design and Characterization of a Bellow-Driven, Self-Sensing, Soft Pneumatic Actuator

Ryman Hashem, Martin Stommel, Leo K. Cheng, *Member, IEEE,* and Weiliang Xu, *Senior Member, IEEE*

***Abstract*—Soft robotics concepts are inspired by how biological organisms behave to their surroundings, for example, physical contractions of a human stomach. Stomach contractions present challenges in design for engineers, which limits the development of a soft robot stomach simulator. We present a novel bellow-driven soft pneumatic actuator (SPA) with a self-sensing capability that generates linear displacement as a solution for applications such as a soft robot stomach simulator. The SPA concept, design, modeling, fabrication and experimental characterization are presented. The SPA consists of several silicones that shape the actuator and influence its performance. A soft bellow is embedded in the SPA, which reacts linearly to pressurizations. The full displacement range of the SPA was 16 mm. Although the proposed SPA is a linear soft actuator, the arrangement of multi-SPAs in a circular body structure can achieve a contraction. The silicone used in the SPA usually exhibits viscoelasticity behavior. A lumped viscoelastic model was employed to predicts the displacement of the SPA from a known applied pressure. The model was successfully validated, which results in a maximum displacement error of 3%. A sensory system was embedded in the SPA for monitoring the displacement. A linear equation calibrated the sensor readings with a displacement error of 2%. The SPA produced a force of 0 to 6 N during the pressurization between -50 to 90 kPa. The results shown the capability of the SPA to be implemented on the soft robot stomach simulator.**

***Index Terms*—Soft robotics, Soft pneumatic actuator, linear soft actuator, viscoelastic model, creep behavior.**

I. Introduction

SOFT robotics is an emerging field that involves the disciplines of robotics, biology, materials and bioengineering [1], [2]. Many soft robots are driven pneumatically by inflating sealed compliant chambers such as soft pneumatic actuators (SPAs) [3]–[6]. SPAs accomplish a delicate and flexible interaction with objects. Linear SPAs extend linearly by one degree of freedom (DoF). Pneumatic artificial muscles are an example of linear SPAs that compress [7], [8]. However, It is challenging to design a miniature linear SPA with a large displacement.

Researchers proposed different methods to obtain a linear displacement from SPAs [9]–[12]. The methods can be narrowed into two main techniques: fiber-reinforced actuators [13], [14] and elastomeric origami actuators [15], [16]. The fiber-reinforced actuator consists of a pneumatic bladder wrapped with fiber wires. The arrangement of fiber-reinforcement specifies the output motion during inflation. The extension of such an actuator achieves slight axial expansion or contraction of the original size. Thus, fiber-reinforced actuators are not used for a large linear expansion [17]. The elastomeric origami actuators consist of a pneumatic chamber and a patterned sheet (e.g., paper or fiber) embedded. The sheet is folded as a 3D structure [15]. It can be challenging to reliably manufacture large quantities of origami sheets less than 1 cm in size. Origami-based actuators obtain a large displacement in response to pneumatic inflation [16]. The technique of origami is viable for large linear displacement actuation if a practical fabrication method is obtained for miniature actuators. Comparable to the origami actuation, silicone bellows provide a linear displacement via retractable folds. Unlike origami, the fabrication of miniature bellows is possible by an injection molding technique. Soft robots that utilize bellows are mainly designed for bending motion as a joint [18] or as a micro-bellows gripper [19]. The design of both actuators can not be implemented for a linear SPA. The proposed bellow-driven SPA is a novel design that is built entirely from soft materials to achieve linear displacement. The linear displacement can be predicted from a known applied pressure through SPA modeling.

Soft robots can be modeled by finite element analysis (FEA) [20] or by quasi-static deformation [21]. The composite design of the SPA makes the modeling of such methods difficult. The deformable layer used in this study is EcoFlex 00-30. Case et al. suggested that EcoFlex 00-30 exhibits viscoelastic behavior [22]. The material presents a continued increase in displacement upon constant loading (creep). A constitutive equation represents such creep with time as a variable [23]. A linear viscoelastic model is introduced to predict the displacement of the SPA. Also, a sensory system is introduced to monitor the displacement.

Soft robotic sensors provide methods to quantify the stretchability of the soft materials [24]. Such methods can be narrowed into two types: stretchable sensors and vision systems. Stretchable sensors are embedded in soft materials for direct interaction. Felt et al. [18] propose an inductance-based sensing system for bellows-driven joints. The disadvantage of this system is the calibration when assembling many SPAs and the large error of 1.3 mm. Vision systems are more accurate with robust technology. Thien et al. tested a gesture sensor to measure the distances of pigmented silicone [25]. The conducted measurements are between 15-25 mm with accurate sensor readings. The results prove the viability of using an

R. Hashem is with the Department of Mechanical Engineering, University of Auckland, Auckland 1010, New Zealand (e-mail: aabo845@aucklanduni.ac.nz).

W. Xu is with the Department of Mechanical Engineering, University of Auckland, Auckland 1010, New Zealand (e-mail: p.xu@auckland.ac.nz)

L. K. Cheng is with the Auckland Bioengineering Institute, University of Auckland, Auckland 1010, New Zealand (e-mail: l.cheng@auckland.ac.nz).

M. Stommel is with the Department of Electrical and Electronic Engineering, Auckland University of Technology, Auckland 1010, New Zealand (e-mail: mstommel@aut.ac.nz).

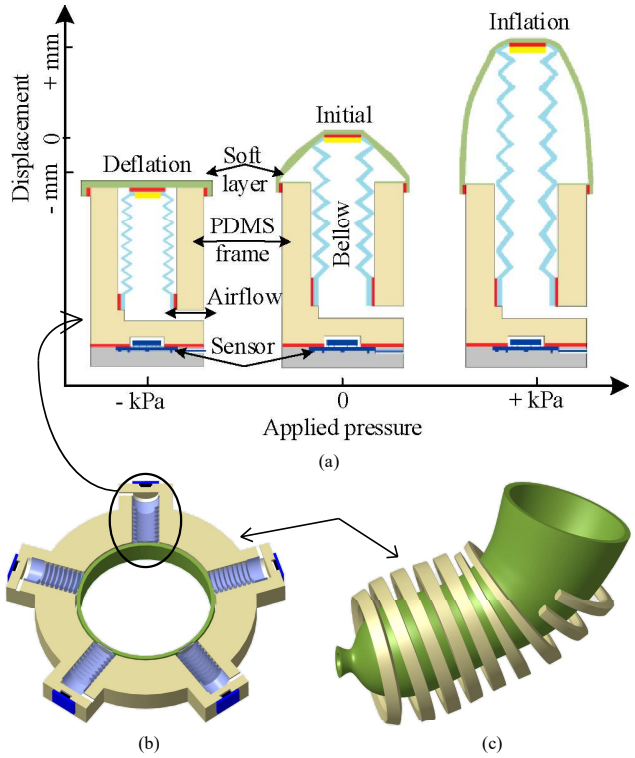

Fig. 1. The conceptual model of the bellow-driven SPA (a) in the deflation state, the initial state and the inflation state. (b) The conceptual model of the bellow-driven ring SPA which consists of multi-SPAs. (c) The conceptual model of the soft robot stomach simulator, which consists of multi-ring SPAs.

IR sensor with soft robots. This sensing concept is adapted in this paper with a range sensor (RS) to accommodate a sensory system for the bellow-driven SPA.

The purpose of developing the bellow-driven SPA is to be fitted in a soft robot stomach simulator that can mimic the contraction of a human stomach. The importance of developing such a robot lies in need of a test environment that can improve the knowledge of digestion in both healthy and diseased stomach such as gastric arrhythmia [26], and advance the research toward food and drugs technologies [27]. The challenge toward developing a stomach robot is highlighted by developing soft ring actuators that contract similar to a human stomach. Dang et al. developed a ring-shaped actuator to mimic the radial contraction in nature [21], [28]; however, the actuator showed a maximum contraction ratio of 30%, which is significantly smaller than a stomach contraction of 80% [29]. In previous work, we proposed the concept of a soft-bodied gastric robot that is capable of mimicking the motility of the human stomach [30]. However, the deformation of the ring actuator exhibited an undesired large width of the contraction [31]. Therefore, the proposed SPA fulfills the specifications of the soft robot stomach simulator by fitting multi-SPAs in a ring structure to perform a contraction similar to a human stomach. Although the proposed actuator is designed for a specific application, it can be a generic model as a linear SPA with a self-sensory system. The proposed SPA can be stacked in the form of a soft table that generates peristaltic deformation, which has been achieved with hybrid linear actuators [32].

TABLE I
THE SPECIFICATION OF A HUMAN STOMACH MOTILITY AND GEOMETRY [29]

Property	Quantity
ACW lifespan	60s
ACW cycle	3cpm
ACW velocity	$\approx 2.5mm/s$
ACW contraction ratio	$30\% - 80\%$
ACW contraction width	≈ 10 to $20mm$
ACW force	$\approx 0.2 - 2N$
ACW pacemaker	$\approx 150mm$ from pylorus
Stomach diameters	$\approx 20mm - 100mm$

This paper demonstrates the use of a linear bellow-driven SPA with a sensory system as a modular soft actuator. The bellow-driven SPA is capable of a linear deformation. An off-the-shelf rang sensor measures the deformation. The conceptual design, modeling, fabrication and validation of the SPA are presented. The conceptual design is presented in Section II. The modeling of the SPA as a linear viscoelastic actuator is described in Section III. The fabrication process of the actuator is described in Section IV. The experimental setup of seven experiments that are conducted to characterize the SPA is explained in Section V. The validation and calibration of the SPA and the RS are presented in Section VI.

II. Specification, Concept and Design of a Bellow-Driven SPA Module

A. Specification of the SPA

The achievement of the anthropomorphic engineering design is formed by simplifications of the biological system [33]. The simplification of a human stomach toward the development of soft robot stomach simulator has three aspects: I) the structure of human stomach as a hollow compliant organ, II) the mode of the stomach motility with a low-frequency wave cycle, and III) the contraction rate of the antral contraction waves (ACW). The ACWs typically traverse with increasing contraction at a speed of $\approx 0.25cm/s$ with a continuous smooth rhythm from the pacemaker (initiation) to the pylorus (termination). The contraction ratio increases to 80% at the end of the contractions, where the diameter of the stomach about 50 mm. The specifications expected for the stomach robot are presented in Table I. A linear SPA is proposed to execute a controllable deformation (displacement of 15 mm and width of 20 mm) that simulates the ACW deformation (see Fig. 1 a). Linear SPAs can achieve a contraction by embedding multi-SPAs in a ring frame (see Fig. 1 b). To perform 80% of contraction from a ring actuator of a diameter of 50 mm, a single SPA should deliver a 15 mm of displacement. The ring actuators will be stacked together to form a stomach robot in future work (see Fig. 1 c). In this work, we focus on the development and characterization of the linear SPA.

TABLE II
SUMMARY OF PARAMETERS

Symbol	Parameter	Symbol	Parameter
A	Effective surface	C	Constant
D	Resulted displacement	D^{ex}	Experimental displacement
D^{fr}	Formulated displacement	E	Young's modulus
ϵ	Elongation of bellows	H	Heaviside function
$\eta_{1,2}$	Kelvin material viscosity	J	Creep compliance
K	Spring rate	$k_{1,2}$	Kelvin material elasticity
M	Bellow convolutions	n	Obtained data points
P_{th}	Pressure thrust	P	Applied pressure
τ_1	Arbitrary time	t	Time
$\vec{V}$	Parameters vector	w	Wall thickness
Z	Mean diameter of bellow		

B. Concept of the SPA

In order to satisfy the specifications mentioned in Table I, a modular approach is followed (see Fig. 1). The actuation of the linear SPA is accomplished by embedding a silicone bellow in a transparent frame with a soft layer attached to the free side of the bellow. The inflation of a bellow by an external pressure source produces a net force to the inner chamber, resulting in a displacement of the SPA. The elasticity of the soft layer and the bellow produces a restoring force once the external pressure is discharged (initial state). A range sensor is employed to detects the displacement of the paint inside the bellow. The sensor controls the intensity of the reflected light from the paint. The conceptual design of the SPA consists of the following four considerations: 1) the SPA is driven by a hollow bellow that it is attached to the frame from the bottom, 2) the deformable soft layer of silicone is attached to the top of the bellow and around the frame, 3) the RS is centered on the base of the frame to measure the displacement through a silicone layer, 4) the frame of the actuator is made out of transparent silicone to allow measurements of the RS.

The bellow proposed in this study consists of thin-walled, hollow silicone cylinders, with deep convolutions. The top of the bellow is sealed, while the base remains open. The top is movable while the bottom is fixed to the frame. The convolutions of a bellow allow displacement in one direction (longitudinal) and reduce the radial deformation.

C. Design of the SPA

The development of a silicone bellow with specific parameters requires the basic knowledge of the bellow functionality. A bellow elongation and retraction operate as a spring. There are two forces present the bellow actuator: 1) restoring force and 2) pressure thrust. The restoring force is derived from Hooke's law ($F = -K\epsilon$). The pressure thrust acting inside the bellow is expressed as [34]

$$P_{th} = \frac{\epsilon E w^3}{2MAZ^2}. \quad (1)$$

Table II lists all the symbols used in this paper. Equation (1) is a design reference for choosing a bellow for the required

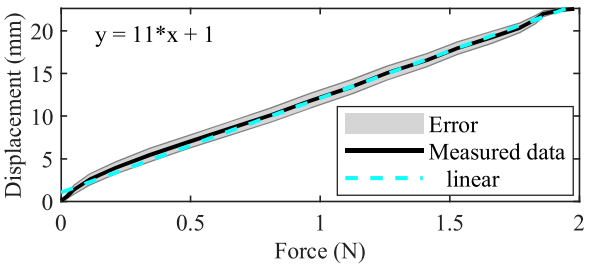

Fig. 2. Force vs. displacement curve for the soft layer of a material mix of Ecoflex 0010 and Slacker with a ratio of 1:0.5.

performance. This equation is not suitable to predict the displacement of an SPA as the bellow is attached with a soft deformable layer. The relationship between the pressure thrust P_{th} and bellow's elongation ϵ is linear. This relationship is disrupted when the elastic limit E of bellow's material is reached, which its occurs during a higher elongation than the total length of a bellow. The number of bellow convolutions M determines the traveling length of a bellow. A larger M provides a larger elongation range.

The soft layer must accommodate the maximum elongation of the bellow, which is 15 mm as specified earlier. A force vs. displacement experiment is employed on a soft layer that validates the elasticity. Fig. 2 shows the experimental result of the displacement of the soft layer upon the applied force. The soft layer can deform up to 22 mm under 2 N of force. Therefore, the soft layer can accommodate the elongation of the bellow, which can be used in the SPA.

The displacement of the SPA is measured by an RS that is fitted under the fixed open side of the bellow and measures the displacement through the frame. The RS demand a transparent wall to function correctly. Therefore, transparent silicone material should be used for the frame. The frame dimensions are designed to accommodate a bellow with a diameter of 10 mm and to limit the horizontal deformation to 20 mm as required in this study.

III. LUMPED VISCOELASTIC MODELING

A. Model formulation

The SPA includes soft materials that exhibit a viscoelastic response [22]. Such a response inherits a creep which can be represented by the available viscoelastic models such as the Kelvin-Voigt model [23]. A Kelvin-Voigt model represents a retarded elastic behavior by spring and viscous elements that are connected in parallel. The retarded elastic behavior is a response where an applied pressure is carried by a viscous element. Then, the load of the stress is transferring to the elastic element. A single Kelvin-Voigt model results in a step response similar to a first order system, which does not fit the response of the SPA. The step response of the SPA exhibits two retarded elastic behavior upon a constantly applied pressure, which are given by the creep compliance of J=J_1+J_2 (see Fig. 3). Each creep compliance represents a retarded elastic behavior. Therefore, the proposed model includes two Kelvin-Voigt elements (four elements) that are connected in series. The model is introduced to predict an output displacement

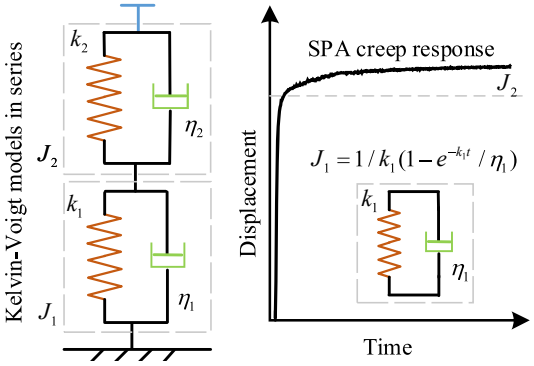

Fig. 3. The linear four-elements viscoelastic model.The model combined two Kelvin-Voigt elements in series to predict the creep response. Each creep compliance (J_1 and J_2) represents a retarded elastic behavior as compared to the SPA response. The Kelvin-Voigt models have elasticity elements $k_{1,2}$ and viscosity elements $\eta_{1,2}$.

$(D(t))$ from a constant or arbitrary applied pressure relating to time (t) according to the equations [23]

$$D(t) = H(t)P * J(t), \tag{2}$$

$$D(t) = \int_0^t J(t-\tau)H(t-\tau)d[P(\tau))], \tag{3}$$

$$J(t) = [1/k_1(1-e^{-k_1 t/\eta_1})] + [1/k_2(1-e^{-k_2 t/\eta_2})], \tag{4}$$

The terms $1/k_1$ and $1/k_2$ are the instantaneous elasticity and recovery. The terms $-k_1 t/\eta_1$ and $-k_2 t/\eta_2$ are the retarded elastic behaviour.

Equation (2) is the displacement response to a Heaviside step function of pressure. Equation (3) is the integration of a continuous displacement response to arbitrarily applied pressure. Equation (4) is the creep compliance for two connected Kelvin-Voigt models in series.

The four elements model is particularly used for a linear response. Therefore, the response of the SPA should hold the linearity law [23]

$$D[CP(t)] = CD[P(t)], \tag{5}$$

The actuation of the SPA may perform nonlinearly from the composite material that constructs the actuator. Equation (5) states the linearity law as a principle to represent the SPA with the linear viscoelastic four elements model.

B. Identification of the four elements

The four parameters of the viscoelastic model are the elastic coefficients $k_{1,2}$ and viscous coefficients $\eta_{1,2}$ (see Fig. 3). The identification of the parameters in the SPA model is based on experimental data. We identify the four parameters by model fitting using a nonlinear least square with Trust-Region algorithm. An objective function

$$f(\vec{V}) = \sum_{n=1}^{n}\sum_{i=1}^{i}\left(\frac{D(V)_i^{fr} - D_i^{ex}}{D_i^{ex}}\right)^2 \tag{6}$$

is defined as the difference between the experimental displacement and the calculated displacement by the model under different applied pressure. The term $\vec{V} = [k_1, k_2, \eta_1, \eta_2]^T$ is the parameters vector which represents the set of the creep variables. The symbols $D(V)^{fr}$ denote the model displacement of the SPA and D^{ex} denote the experimentally measured displacement. The index i is the variable of time of the experiment, while the index n represents the variable of several SPA step responses with different applied pressure.

The initial guess of parameters is obtained by a curve fitting tool in MATLAB ($cftool$) that fits a step response with constant pressure. The optimized parameters of different applied pressure are derived by an optimization tool ($fmincon$).

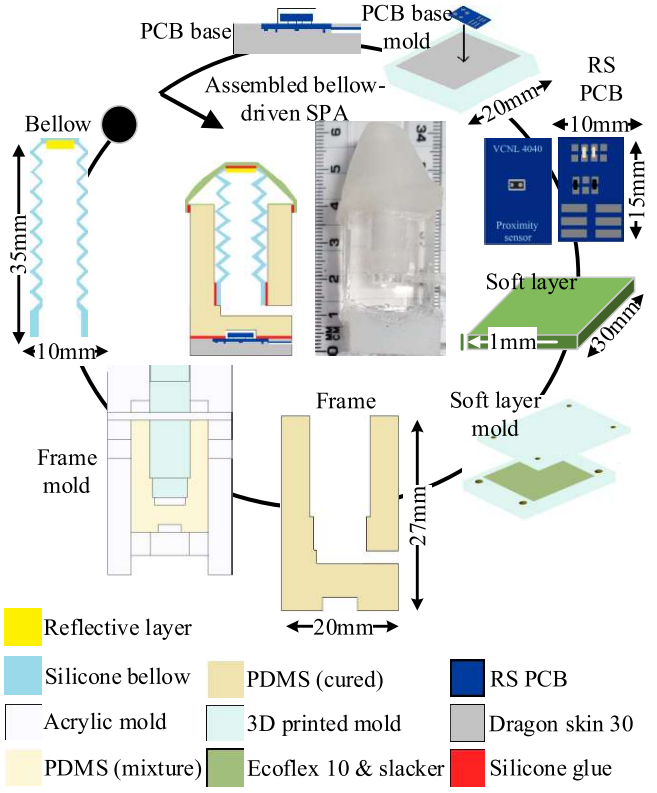

Fig. 4. The fabrication process of a bellow-driven SPA. The assembly is arranged by the molded parts.The circular bottom of a bellow (5 mm height) is glued to its fit in the PDMS base. The soft layer is centered and is glued with the top of the bellow. The soft layer edges are glued on the outer side of the frame wall. A channel is drilled on the side of the PDMS base for an airflow. The PCB is fitted in the mold with a silicone mixture. The sensor base is glued to the actuator frame.

IV. Fabrication of a Bellow-driven SPA

A schematic illustration of the fabrication process of the SPA is shown in Fig. 4. The geometry of the SPA is designed with specifications that are required for the soft robot stomach simulator [28], [30]. The bellow has a dimension of a total height of 35 mm, a deformable height of 15 mm, a wall thickness of 0.8 mm, an outer diameter of 10 mm, an inner diameter of 5 mm, and eight deformable convolutions of the bellow. An injection molding process manufactures the bellow from translucent silicone with a strength of Shore 50 A. White silicone pigment (Silc Pig, Smooth-On) is internally added to the bellow to reflect IR sensor signals.

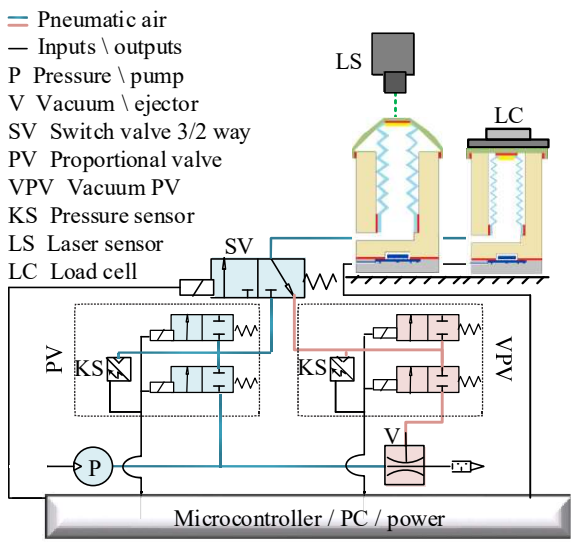

Fig. 5. Experiment set-up for the bellow-driven SPA.

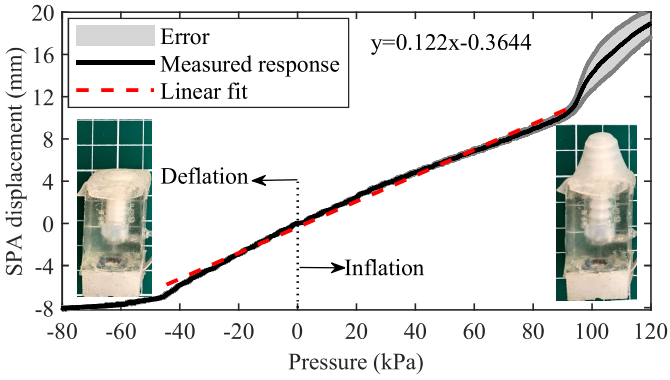

Fig. 6. The full displacement range of the SPA during actuation. The SPA achieves a linear displacement between -7 to 9 mm (-50 to 90 kPa). The linear regression is the calibration of the displacement upon pressurization. The linear regression is fitted with a displacement error of 2%. Above the 2% error, it is considered a nonlinear error that is shown in two segments between -80 to -50 kPa and 90 to 120 kPa. The SD of the linear segment is $\pm$ 0.2 mm. The quality of the linear regression is $R^2 = 0.99$.

The formation of the soft layer is created by mixing room temperature vulcanization (RTV) silicone and a softener (Ecoflex 0010 and Slacker, Smooth-On, Easton, PA, USA). The mix ratio of the Ecoflex 0010 and Slacker is 1:0.5. The fabrication technique is molding and casting. The thickness of the soft layer is 1 mm, and the area is 30 x 30 mm. The mixture is placed in a vacuum to eliminate bubbles, which minimize the fabrication error.

The selected RS is a VCNL4040 (manufactured by VISHAY semiconductors). Its size is 4x2x1 mm. The RS produces calibrated and filtered readings in counts (cts), which are based on the intensity of the reflected infrared light. A double-sided PCB is designed for the RS with a size of 15 x 10 mm.

The frame material is chosen to be Polydimethylsiloxane (PDMS, Sylgard 184 Dow Corning) for its transparency and high Young modulus. The transparency of this material is essential for the sensing system. The hardness of the material (Shore 50 A) is necessary as a frame. Accordingly, the frame can be regarded as rigid. The fabrication of the frame is created by the molding and casting method. The mold is made of acrylic sheets to achieve a flat and smooth surface, which improves the clarity of a cured PDMS frame. The PCB base is made of silicone material (Dragonskin Smooth-On). Silicone adhesive is used for the assembly of separate parts.

V. Experimental Setup

The characterization of the actuator involves seven experiments ($Ex_{1..7}$). The first experiment (Ex_1) aims to achieve the full displacement capability of the SPA. For modelling the SPA, the linear range of the displacement is required. The actuation of the SPA (deflation and inflation stages) is produced via a ramp function of applied pressure. The range of applied pressure is from -80 to 120 kPa.

The aim of Ex_2 is to conduct the resulted forces generated on the SPA surface and compare it with the actuator specification. In Ex_2, the actuator is fully retracted and blocked by a load cell during actuation (blocking force). The blocking force of the SPA is achieved by applying a ramp function of applied pressure similar to Ex_1 while the load cell is recording measurements in Kg. The measurement is converted to newton.

Ex_3 is conducted to verify if the actuation of the SPA is a linear viscoelastic system as presented in (5). The experiment compares three points of different applied pressure at a given time. The different applied pressure are performed by step responses technique.

Two experiments ($Ex_{4,5}$) are conducted to optimize the parameters of the model ($k_{1,2}, \eta_{1,2}$). The initial guess of the parameters is represented by curve fitting a step response (from (2)) in Ex_4. Seven step responses (-20 to 50 kPa with 10 kPa increment) are used in the optimization algorithm to estimate the values of the parameters in Ex_5.

The viscoelastic model is validated by Ex_6, where the proposed model is compared with measured data via the step function of applied pressure from (3).

The RS is tested and calibrated in Ex_7 with a ramp function of applied pressure similar to Ex_1. Also, the linear range of the RS readings is related to the linear range of the displacement.

The experiments are carried out using the setups shown in Fig. 5. The following electro-pneumatic system drives the SPA. A 3/2 way solenoid valve (SV, 005 series microvalve, Koganei) is used to switch between deflation and inflation states. A proportional solenoid valve (PV, ITV0030, SMC) with a built-in pressure sensor (KS) is employed for the inflation state through an air pump. A proportional solenoid valve (VPV, ITV0090, SMC) with a built-in KS is utilized for the deflation state through a vacuum ejector (V, ZK2A12K5RW-08, SMC). A master microcontroller (myRIO) is used to control the solenoid valves and to receive RS readings. The PCB of the RS communicates with myRIO through an I^2C bus. The control program is written in LabVIEW (National Instruments) to control both inflation and deflation states. The built-in KS has an error of 0.5 kPa; therefore, the error is neglected. A commanded pressure is given to the control system in all experiments, while the feedback from the built-in KS utilizes a PID controller of both PV and VPV.

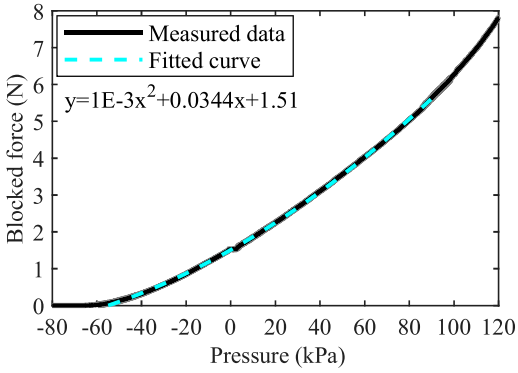

Fig. 7. The blocking force of the SPA over an applied ramp function of applied pressure. The fixed load cell is recording the blocking force during actuation. The fitted curve is a second order nonlinear polynomial. The measured data is the mean from 10 repeated tests with 0.1 N of SD. The quality of the fitted curve is $R^2 = 0.99$.

$Ex_{1,2,4,5,6,7}$ employ a laser sensor (Wenglor OPT2001 distance measuring) to measure the displacement of the SPA as the sensor is centered on the soft layer. Also, the laser sensor is used to characterize the RS readings. Ex_3 applies a load cell (Beam load cell, TAL220) to measure the blocking force. The load cell is fixed over a plate that blocks the SPA from displacement. The load cell is placed at the full retraction state of the SPA (see Fig. 5). All data are acquired at 20 Hz. All experiments are repeated ten times to obtain sufficient data for computing the mean and the standard deviation (SD). The results of the tests are described by fitted curves. The quality of the fitted curves is defined by the coefficient of determination (R^2) with a range from 0 to 1, which 1 means perfect fitting.

VI. Results

Fig. 6 shows the result of the full range of SPA displacement (Ex_1). A linear and nonlinear displacement segments are distinguished from the result by linear regression with an acceptable displacement error of 2%. The linear displacement segment is between a minimum length of -7 mm at (≈-50 kPa) and a maximum length of 9 mm at (≈ 90 kPa). The standard deviation of the linear segment is ± 0.2 mm, which implies good repeatably of the SPA. During the retraction state (from 0 to -50 kPa), the nonlinearity is higher than the inflation state. That is because the deflation state has more frictional force between the bellow and the frame wall. The linear regression is the calibration of the SPA displacement upon pressurization in Fig. 6. The calibration is represented by a linear equation $P = L*x+g$, where L represents the slope, x is the measured displacement (mm), and g is the offset of the applied pressure (kPa). The total linear displacement of the bellow-driven SPA is 16 mm. Above 2% of displacement error is out of the linear regression range, so it is considered nonlinear deformation.

The nonlinear sections appear during deflation after the full retraction of the bellow and during inflation after the maximum elongation allowed (elastic limit) of the bellow. The standard deviation of the nonlinear sections is ± 1.5 mm. The nonlinear segments are ignored in this work.

Fig. 7 shows the result of the blocking force of the SPA (Ex_2). The measured data exhibits a minimal SD of ± 0.1 mm.

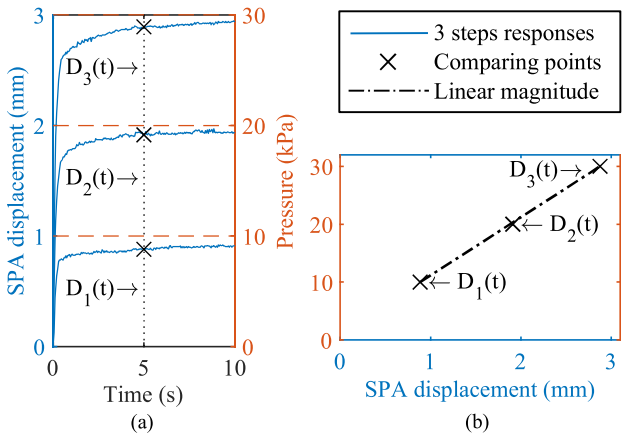

Fig. 8. The viscoelastic linearity test of the SPA actuation response. (a) Three constant pressures (10, 20 and 30 kPa) applied at time 0 to 10 s which produce three time-dependent displacements responses ($D_1(t)$, $D_2(t)$, and $D_3(t)$), three points are set on the three responses at 5 s. (b) The comparison of the three points at 5 s illustrates a proportional relationship between displacements and applied pressures by a linear magnitude. The displacement error is 0.1 mm. The linear magnitude implies that the SPA response can be represented by a linear viscoelastic model.

TABLE III
Viscoelastic four parameters model values

Estimation method	k_1	k_2	η_1	η_2
Initial (curve fitted by cftool)	107.1	11.96	1029	1.784
Final (optimized by fmincon)	82.85	11.45	345.6	2.036

A second order polynomial represents the result with a residual error of 0.2 N. The output force is fitted with $R^2 = 0.99$. The range of the output force is focused on the linear segment of the SPA displacement: 0.2 N at -50 kPa to 6 N at 90 kPa (see Fig. 7). Therefore, the SPA can move an object up to 0.6 Kg.

The viscoelastic linearity test (Ex_3) is presented in Fig. 8. Fig. 8(a) displays three points that are used in (3). Fig. 8b shows the proportional relationship between the displacement and applied pressure of the three compared points. The linear magnitude in Fig. 8b exhibits a displacement error from $D_{1,2,3}$ of ≈ 0.1 mm. Equation (3) applies to the SPA, where the pressure is proportional to the displacement at a given time. Therefore, a linear viscoelastic model describes the SPA.

The initial parameters of the model are abstracted from a fitted curve that is shown in Fig. 9a (Ex_4). The fitted curve is matched with the measured displacement response with an $R^2 = 0.99$ and a minor displacement error of 0.05 mm. The result of Ex_5 is shown in Fig. 9b. The SD of the repeated experiments is $\pm 0.2mm$. The initial and optimized parameters of the model from $Ex_{4,5}$ are presented in Table III. The optimized parameters are successfully fitted with $R^2 = 0.97$.

The viscoelastic four elements model's validation (Ex_6) is illustrated in Fig. 9c. The proposed model (with the optimized parameters values) is compared with the measured SPA actuation responses against a step function of applied pressure that

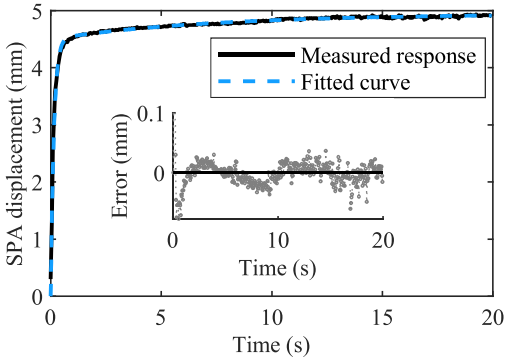

(a)

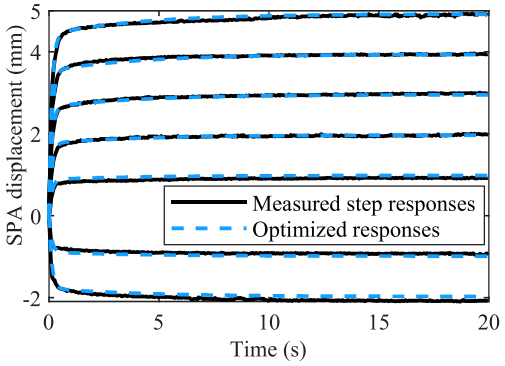

(b)

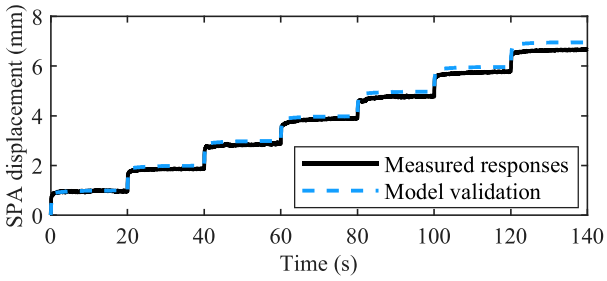

(c)

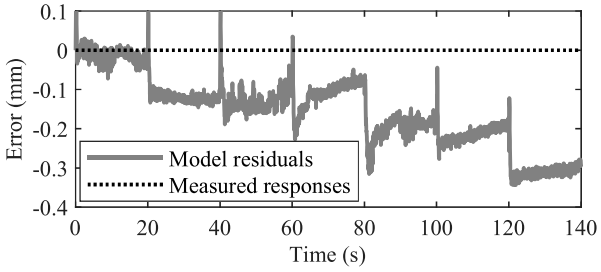

(d)

Fig. 9. The results of $Ex_{4,5,6}$ that provide the initial parameters, optimized parameters and the validation of the four elements model. (a) The curve fitting of the viscoelastic model on a constant 50 kPa step response to obtain the initial four parameters. The fitted curve has an error of 0.05 mm. (b) The optimization of the viscoelastic model on step responses of applied pressure between -20 to 50 kPa (by 10 kPa increments) to obtain the optimized four parameters. The quality of the fitted responses is $R^2 = 0.97$. (c) The validation of the four elements model is described by the comparison of the measured responses and the model responses. An increment of applied pressure from 10 to 70 kPa (0.05 Hz) is employed. (d) The residuals of the validation result with a displacement error of 0.3 mm.

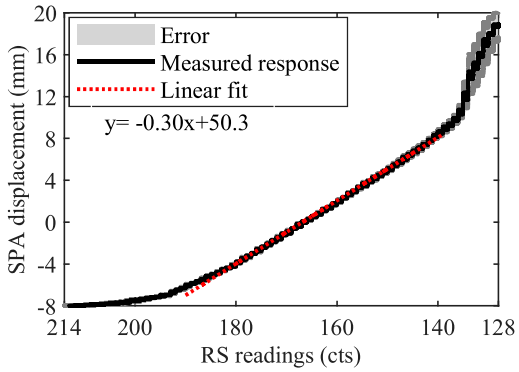

Fig. 10. The full range of the RS detection of the SPA deformation. The RS readings follow the SPA displacement with two segments (linear and nonlinear). The linear segment is between -7 and 9 mm. The linear segment is represented by a linear regression, which serves as the calibration of the RS readings upon the displacement. The linear regression is fitted with an allowable RS readings error of 2%. The SD of the repeated tests is ± 2 cts. The quality of the linear regression is $R^2 = 0.99$.

is generated from (5). The model predicts the displacement with a maximum displacement error of 0.3 mm (see Fig. 9d) and $R^2 = 0.98$. The displacement error progresses nonlinearly by increasing the applied pressure. This behavior occurs as the inherent nonlinearity of the soft layer is raised upon excessive tensile stress. The proposed model has a low displacement error of less than 5%. Therefore, the model is valid for open-loop control of the SPA. For monitoring the displacement of the SPA, the RS is introduced.

Fig. 10 presents the range of the RS readings regarding the displacement of the SPA (Ex_7). As the RS readings track the SPA displacement significantly, a linear and a nonlinear displacement is presented that is similar to the result of Ex_1. The linear segment of the RS readings is between a minimum length of -7 mm and a maximum length of 9 mm. The SD of the linear segment is $\pm$ 0.5 mm, which proves the repeatability and the compatibility of the RS as a sensor for the SPA. The linear regression of the RS readings is fitted with quality of $R^2 = 0.98$. The calibration of the RS readings upon the displacement is characterized by a linear equation $S = L * x + f$, where S is the displacement of the SPA in mm, x is the sensor readings in cts, and f is the offset of the sensor readings in cts. The offset value depends on the thickness of the PDMS that is placed on the top of the sensor. The result validates the use of the RS as a sensory system that detects the displacement of the soft actuator.

VII. Discussion and Conclusion

We presented a bellow-driven SPA combined with a displacement sensory system. The SPA performed a linear displacement of 16 mm, which exceeds the required 15 mm for the gastric application. The response of the SPA is nonlinear for displacement greater than 16 mm as the linear limit of the bellow is reached. The soft layer can deform up to 22 mm, which meets the design requirements in maximum displacement. The fabrication of the soft layer with a 1 mm thickness must be accomplished with a minor fabrication error by removing the bubbles during casting, as such an error provides

different deformation characteristics. The displacement of the SPA of 16 mm can achieve a required contraction of 80% when multi-SPAs embed in a ring frame of 50 mm. Therefore, the SPA is adequate for the stomach robot application.

The maximum force of the SPA is 6 N. The generated force by the SPA can be altered by changing the wall thickness of a bellow (w), which is proportional to the applied pressure from (1). In this work, the generated force is sufficient for the soft actuation required from the SPA.

The SPA was successfully modeled by the four elements viscoelastic model to predict the displacement with the inherent creep upon a known applied pressure. The validation of the experiment showed a maximum error of 0.3 mm (about 3%) of predicted displacement. The minor displacement error proves the viability of the model to represent the actuator in an open-loop control system. The limitation of the model is that it works only for linear systems, while most of the soft robots behave nonlinearly.

The RS system provided excellent performance in measuring the displacement of the SPA by a linear equation with an allowable sensor readings error of ± 0.5 mm. The sensory system showed an excellent result with a 40% reduction of displacement error compared to the inductance-based sensing system for bellows-driven joint with a 1.3 mm error [18]. As embedded in the actuator, the sensor is capable of detecting the displacement of an enclosed application. Therefore, the sensory system is a valid method for detecting the displacement of the SPA while placed on the soft robot stomach simulator.

ACKNOWLEDGMENT

The work presented in this paper was funded by the Medical Technologies Centre of Research Excellence (MedTech CoRE), New Zealand.

REFERENCES

[1] D. Rus and M. T. Tolley. Design, fabrication and control of soft robots. *Nature*, 521(7553):467–475, 2015.

[2] M. Calisti, G. Picardi, and C. Laschi. Fundamentals of soft robot locomotion. *J. Royal Soc. Interface*, 14(130):20170101, 2017.

[3] B. A. Trimmer, H. T Lin, A. Baryshyan, G. G. Leisk, and D. L. Kaplan. Towards a biomorphic soft robot: Design constraints and solutions. In *Biomedical Robotics and Biomechatronics*, pages 599–605, 2012.

[4] R. F. Shepherd, F. Ilievski, W. Choi, S. A. Morin, A. A. Stokes, A. D. Mazzeo, X. Chen, M. Wang, and G. M. Whitesides. Multigait soft robot. *PNAS*, 108(51):20400–20403, 2011.

[5] R. V. Martinez, A. C. Glavan, C. Keplinger, A. I. Oyetibo, and G. M. Whitesides. Soft actuators and robots that are resistant to mechanical damage. *Adv. Funct. Mater.*, 24(20):3003–3010, 2014.

[6] H. Lipson. Challenges and opportunities for design, simulation, and fabrication of soft robots. *Soft Robotics*, 1(P):21–27, 2013.

[7] S. Li, D. M. Vogt, D. Rus, and R. J. Wood. Fluid-driven origami-inspired artificial muscles. *PNAS*, 114(50):13132–13137, 2017.

[8] E. H. Skorina, M. Luo, W. Y. Oo, W. Tao, F. Chen, S. Youssefian, N. Rahbar, and C.D. Onal. Reverse pneumatic artificial muscles (rpams): Modeling, integration, and control. *PloS one*, 13(10):e0204637, 2018.

[9] C. Laschi, M. Cianchetti, B. Mazzolai, L. Margheri, M. Follador, and P. Dario. Soft robot arm inspired by the octopus. *Advanced Robotics*, 26(7):709–727, 2012.

[10] M. Cianchetti, M. Calisti, L. Margheri, M. Kuba, and C. Laschi. Bioinspired locomotion and grasping in water: the soft eight-arm octopus robot. *Bioinspiration Biomim*, 10(3):035003, 2015.

[11] T. Nakamura and K. Suzuki. Development of a peristaltic pump based on bowel peristalsis using artificial rubber muscle. *Advanced Robotics*, 25(3-4):371–385, 2011.

[12] P. Moseley, J. M. Florez, H. A. Sonar, G. Agarwal, W. Curtin, and J. Paik. Modeling, design, and development of soft pneumatic actuators with finite element method. *Adv. Eng. Mater.*, 2015.

[13] F. Connolly, C. J.Walsh, and K. Bertoldi. Automatic design of fiber-reinforced soft actuators for trajectory matching. *PNAS*, 114(1):51–56, 2017.

[14] P. York, T. Clites, E. Boggs, R. Neff, P. Polygerinos, D. Holland, L. Stirling, K. Galloway, C. Wee, and C. Walsh. Biologically inspired soft robot for thumb rehabilitation. *Journal of Medical Devices*, 8(2):020933, 2014.

[15] D. Rus and M. T. Tolley. Design, fabrication and control of origami robots. *Nature Reviews Materials*, 3(6):101, 2018.

[16] R. V. Martinez, C. R. Fish, X. Chen, and G. M. Whitesides. Elastomeric origami: programmable paper-elastomer composites as pneumatic actuators. *Adv. Funct. Mater*, 22(7):1376–1384, 2012.

[17] J. T. Overvelde K. C. Galloway R. J. Wood K. Bertoldi P. Polygerinos, Z. Wang and C. J.Walsh. Modeling of soft fiber-reinforced bending actuators. *IEEE Trans. Robot.*, 31(3):778–789, 2015.

[18] W. Felt, M. J. Telleria, T. F. Allen, G. Hein, J. B. Pompa, K. Albert, and C. D. Remy. An inductance-based sensing system for bellows-driven continuum joints in soft robots. *Autonomous Robots*, pages 1–14, 2017.

[19] H. W. Kang, I. H. Lee, and D. W. Cho. Development of a micro-bellows actuator using micro-stereolithography technology. *Microelectronic Engineering*, 83(4-9):1201–1204, 2006.

[20] Y. Elsayed, A. Vincensi, C. Lekakou, T. Geng, C. Saaj, T. Ranzani, M. Cianchetti, and A. Menciassi. Finite element analysis and design optimization of a pneumatically actuating silicone module for robotic surgery applications. *Soft Robotics*, 1(4):255–262, 2014.

[21] Y. Dang, M. Stommel, L. K. Cheng, and W. Xu. A soft ring-shaped actuator for radial contracting deformation: Design and modeling. *Soft Robotics*, 2019. In press.

[22] J. C. Case, E. L. White, and R. K. Kramer. Soft material characterization for robotic applications. *Soft Robotics*, 2(2):80–87, 2015.

[23] W. N. Findley, J. S. Lai, and K. Onaran. *Creep and Relaxation of Nonlinear Viscoelastic Materials - With an Introduction to Linear Viscoelasticity*. Dover Publications, 1976.

[24] H. Wang, M. Totaro, and L. Beccai. Toward perceptive soft robots: Progress and challenges. *Advanced Science*, 5(9):1800541, 2018.

[25] H. Thien, M. Stommel, F. L. Daheron, A. L. Page, Z. Deng, and W. Xu. Embedded infrared imaging to measure the deformation of a soft robotic actuator. In *International Conference, IVCNZ*, pages 1–6. IEEE, 2016.

[26] LK Cheng, P Du, and G O'Grady. Mapping and modeling gastrointestinal bioelectricity: from engineering bench to bedside. *Physiology*, 28(5):310–317, 2013.

[27] S. Blanquet-Diot, S. Denis, S. Chalancon, F. Chaira, J. Cardot, and M. Alric. Use of artificial digestive systems to investigate the biopharmaceutical factors influencing the survival of probiotic yeast during gastrointestinal transit in humans. *Pharmaceutical research*, 29(6):1444–1453, 2012.

[28] Y. Dang, L. K. Cheng, M. Stommel, and W. Xu. Technical requirements and conceptualization of a soft pneumatic actuator inspired by human gastric motility. In *23rd International Conference, M2VIP*, pages 1–6, Nov 2016.

[29] M. A. Kwiatek, A. Steingoetter, A. Pal, D. Menne, J. G. Brasseur, G. S. Hebbard, P. Boesiger, M. Thumshirn, M. Fried, and W. Schwizer. Quantification of distal antral contractile motility in healthy human stomach with magnetic resonance imaging. *Journal of Magnetic Resonance Imaging*, 24(5):1101–1109, 2006.

[30] R. Hashem, W. Xu, M. Stommel, and L. Cheng. Conceptualisation and specification of a biologically-inspired, soft-bodied gastric robot. In *23rd International Conference, M2VIP*, pages 1–6, Nov 2016.

[31] R. Hashem, W. Xu, M. Stommel, and L. K. Cheng. Fea evaluation of ring-shaped soft-actuators for a stomach robot. In *5th International Conference, RITA*, pages 475–487. Springer, 2017.

[32] R. Hashem, B. Smith, D. Browne, and W. Stommel, M.and Xu. Control of a soft-bodied xy peristaltic table for delicate sorting. In *IEEE 14th International Workshop, AMC*, pages 358–363, 2016.

[33] R. Pfeifer, M. Lungarella, and F. Iida. The challenges ahead for bio-inspired'soft'robotics. *Communications of the ACM*, 55(11):76–87, 2012.

[34] J. F. Wilson. Mechanics of bellows: A critical survey. *International Journal of Mechanical Sciences*, 26(11):593 – 605, 1984.